ACS APPLIED MATERIALS & INTERFACES

Research Article

Cite This: ACS Appl. Mater. Interfaces XXXX, XXX, XXX−XXX

www.acsami.org

Microfluidic-Based Genosensor To Detect Human Papillomavirus (HPV16) for Head and Neck Cancer

Andrey Coatrini Soares,[†] Juliana Coatrini Soares,[†] Valquiria Cruz Rodrigues,[†] Heveline Dal Magro Follmann,[‡] Lidia Maria Rebolho Batista Arantes,[§] Ana Carolina Carvalho,[§] Matias Eliseo Melendez,[§] José Humberto T. G. Fregnani,[§] Rui Manuel Reis,[§,∥,⊥] André Lopes Carvalho,[§] and Osvaldo N. Oliveira, Jr.*[,†]

[†]São Carlos Institute of Physics, University of São Paulo, 13566-590 São Carlos, Brazil

[‡]Department of Chemistry, State University of Maringá, 87020-900 Maringá, Brazil

[§]Molecular Oncology Research Center, Barretos Cancer Hospital, 14784-400 Barretos, Brazil

[∥]Life and Health Sciences Research Institute (ICVS), School of Health Sciences, University of Minho, 4710-057 Braga, Portugal

[⊥]ICVS/3B's—PT Government Associate Laboratory, 4710-057 Braga, Portugal

Supporting Information

ABSTRACT: High-risk human papillomavirus (HPV) infection, mainly with HPV16 type, has been increasingly considered as an important etiologic factor in head and neck cancers. Detection of HPV16 is therefore crucial for these types of cancer, but clinical tests are not performed routinely in public health systems owing to the high cost and limitations of the existing tests. In this article, we report on a potentially low-cost genosensor capable of detecting low concentrations of HPV16 in buffer samples and distinguishing, with high accuracy, head and neck cancer cell lines according to their HPV16 status. The genosensor consisted of a microfluidic device that had an active layer of a HPV16 capture DNA probe (cpHPV16) deposited onto a layer-by-layer film of chitosan and chondroitin sulfate. Impedance spectroscopy was the principle of detection utilized, leading to a limit of detection of 10.5 pM for complementary ssDNA HPV16 oligos (ssHPV16). The genosensor was also able to distinguish among $HPV16^{+}$ and $HPV16^{-}$ cell lines, using the multidimensional projection technique interactive document mapping. Hybridization between the ssHPV16 oligos and cpHPV16 probe was confirmed with polarization-modulated infrared reflection-absorption spectroscopy, where PO_2 and amide I and amide II bands from adenine and thymine were monitored. The electrical response could be modeled as resulting from an adsorption process represented in a Freundlich model. Because the fabrication procedures of the microfluidic devices and genosensors and the data collection and analysis can be implemented at low cost, the results presented here amount to a demonstration of possible routine screening for HPV infections.

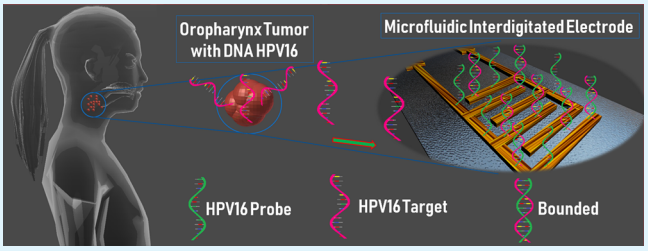

KEYWORDS: *genosensors, HPV, head and neck cancer, impedance spectroscopy, layer-by-layer films, multidimensional projections*

1. INTRODUCTION

Head and neck squamous cell carcinomas (HNSCC) are among the 10 most common human malignancies, exhibiting high rates of morbidity and mortality. The annual worldwide incidence is approximately 740 000 cases, causing 300 000 deaths[1,2] related to tumors in the oral cavity, oropharynx, nasopharynx, hypopharynx, and larynx, more than 90% of which are squamous cell carcinomas.[3,4] Smoking and alcoholism are the major risk factors associated with these tumors. However, human papillomavirus (HPV) infection has recently gained relevance in oropharyngeal tumors because HPV-positive tumors tend to have an improved outcome.[5,6] This detection is still not routinely performed because current techniques for HPV detection are laborious, are costly, have false positives, and/or have difficulties in the quantification of HPV subtypes.[7] These difficulties have motivated research into nanotechnology to manufacture low-cost, fast-detection biosensors to assist in the control of viral epidemics caused by HPV viruses.[8]

In this work, genosensors (which convert the probe-oligos biorecognition into a measurable signal)[9] with impedance spectroscopy as the principle of detection were produced using the layer-by-layer (LbL) deposition method.[10−12] Microfluidic interdigitated electrodes were functionalized with polymeric architectures of chitosan (CHT) and chondroitin sulfate (CS) for DNA probe anchoring to detect HPV16-infected HNSCC cell lines. The choice of CHT and CS as a matrix to immobilize the DNA probe was motivated by two main

Received: August 24, 2018
Accepted: October 8, 2018
Published: October 8, 2018

DOI: 10.1021/acsami.8b14632
ACS Appl. Mater. Interfaces XXXX, XXX, XXX−XXX

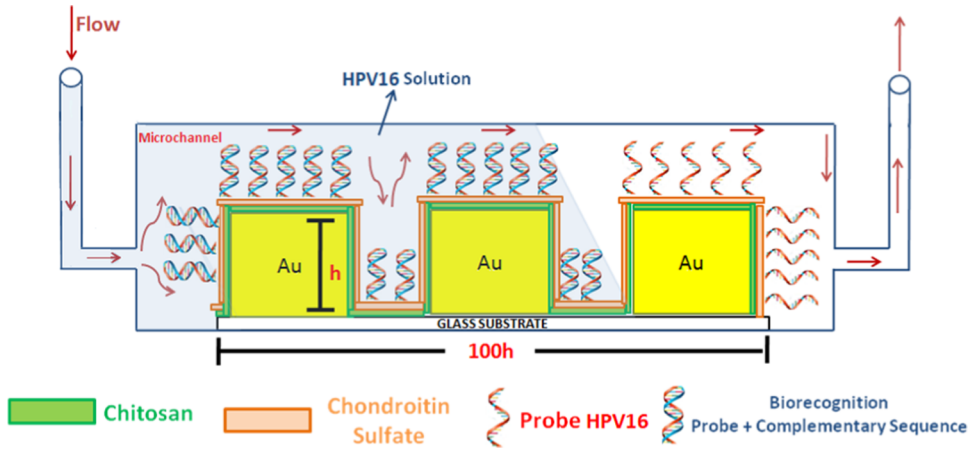

Figure 1. Schematic representation of the functionalization of the electrode and detection of HPV16 under continuous flow.

reasons. These materials have been combined in several tissue engineering applications as scaffolds for cell regeneration because of their biocompatibility, though, to our knowledge, they have not been used in analytical devices. One may therefore expect that CHT/CS layers can preserve the activity of biomolecules in solid films, being amenable for sensors that may be wearable or even implantable. Furthermore, CS possesses carboxylate groups, which permit efficient formation of LbL films via electrostatic interactions with chitosan as well as activation with *N*-hydroxysuccinimide/1-ethyl-3-(3-dimethylaminopropyl)carbodiimide (EDC/NHS) to anchor the HPV16 capture DNA probe (cpHPV16).

2. EXPERIMENTAL SECTION

2.1. Fabrication of Microfluidic Chips. Microfluidic interdigitated electrodes were manufactured with conventional photolithography, in which BK7 glass slides received an initial chemical treatment with hexamethyldisiloxane and positive photoresist AZ4210 deposited by spin coating. The electrodes were then made from a lithographic mask and exposed to UV light for 10 s for photoresist polymerization followed by treatment with tetrabutylammonium hydroxide and metallization via sputtering with chrome and gold. The metalized slides were immersed in acetone to remove the metal deposited on the photoresist. The microchannels in poly-(dimethylsiloxane) (PDMS) were constructed from a SU-8 template. First, PDMS was prepared from the Sylgard 184 kit containing the elastomer silicone and a curing agent, which were mixed and placed in the SU-8 cast, followed by fixation of the silicon capillary. The PDMS microchannels were removed from the cast and sealed on the interdigitated electrodes with O_2 plasma chamber at a pressure of 0.07 torr at 100 W.

2.2. Functionalization of Microfluidic Chips with Nanostructured Films. The LbL technique[10,13,14] was used in coating microfluidic chips with two bilayers of CHT (DD = 85%, M_v = 8.7 × 10^4 g/mol, from Golden-Shell Biochemical, China) and CS (M_v = 2.2 × 10^4 g/mol, from Solabia, Brazil). The step-by-step modification of the microfluidic electrodes is described in the following items:

(1) A 1 mg/mL CHT solution in acetate buffer saline at pH 4.5 and room temperature was injected into the chip microchannel with a microsyringe (Hamilton) and a syringe pump (New Era Pump Syringes) with a flow rate of 20 μL/min for 10 min. This was followed by washing with acetate buffer saline under the same conditions for the removal of poorly adsorbed molecules.

(2) A 1 mg/mL CS aqueous solution was injected into the microchannel under the same conditions as for the first CHT layer, with flow rate of 20 μL/min during 10 min. A washing step followed to remove poorly adsorbed molecules.

(3) Upon repeating steps 1 and 2 above, a two-bilayer LbL film was formed, which then had the carboxylic groups (−COOH) on the CS layer exposed. These groups were activated by injecting a mixed solution of 0.1 M NHS and 0.1 M EDC (Sigma-Aldrich)[15] at 8.3 μL/min during 30 min at room temperature.

(4) With activation in step 3, a stable covalent binding could be established between CS and cpHPV16 probe [NH_2-C_6]-CAAGCAGAACCGGACAG (Sigma-Aldrich), which was deposited next.[16] The cpHPV16 probe sequence, adapted from Arantes et al., 2015,[16] was injected from an aqueous solution into the microchannel interdigitated electrodes at a flow rate 12.5 μL/min during 30 min. In Arantes et al. (2015), a set of three sequences were used together in one polymerase chain reaction (PCR) reaction. Two of those sequences worked as primers for the DNA polymerase. The third sequence (commonly named as "probe") had a 5′ 6-FAM fluorophore and 3′ MGB-NFQ quencher. In our study, the DNA sequence of the probe described by Arantes et al. (2015) was "adapted" because both fluorophore and quencher were eliminated. Then, a 5′ NH_2−C_6 group was added to the cpHPV16 probe. Otherwise, the DNA sequence of our cpHPV16 and the probe from Arantes et al. (2015) are identical. The cpHPV16 probe is responsible for the biorecognition of the complementary ssDNA HPV16 (ssHPV16) positive control, as indicated schematically in Figure 1.

2.3. Description of Cancer Cell Lines. DNA samples from the cell lines CasKi, SiHa, UM-SCC47, UM-SCC104, 93-VU147T, JHU12, JHU13, and JHU28 were analyzed using electrical impedance measurements with the biosensors manufactured as described in Sections 2.1 and 2.2. The human cancer cell lines SiHa and CaSki were acquired from the American Type Culture Collection. Cell lines UM-SCC47 and UM-SCC104 were acquired from Millipore (Cat. # SCC071 and Cat. # SCC072, respectively). 93-VU147T was kindly provided by Dr. Josephine Dorsman (VU University Medical Center) and JHU12, JHU13, and JHU28 were kindly provided by Dr. Joseph Califano (Johns Hopkins University). These cell lines were maintained in Dulbecco's modified Eagle's medium or RPMI 1640 containing 10% fetal bovine serum, 1% penicillin/streptomycin, and 2 mM glutamine in a humidified 5% CO_2 incubator at 37 °C. Genomic DNA was isolated from cell culture using QIAamp DNA MicroKit (Qiagen) following the manufacturer's recommendations. The HPV^+ cervical cancer cell lines CasKi and SiHa have 600 and 2 copies of HPV16 per cell, respectively, and were used as positive controls in the experiments using DNA from cell lines. The HPV16 copy number in HNSCC cell lines was determined by qPCR.[16] Head and neck cell lines JHU12, JHU13, and JHU28 were confirmed negative for HPV16, whereas the viral copy number obtained for the HPV^+ cell lines UM-SCC47, UM-SCC104, and 93-VU147T was 33, 2, and 68,

DOI: 10.1021/acsami.8b14632
ACS Appl. Mater. Interfaces XXXX, XXX, XXX−XXX

respectively (Table 1). The number of human genome copies used in experiments was calculated following eq 1

$$N_{\text{copies}} = \frac{\text{amount} \times 6.022 \times 10^{23}}{\text{length} \times 1 \times 10^{9} \times 650} \quad (1)$$

Table 1. Total HPV16 Copies and HPV16 Copies/Human Genome of Seven Cancer Cell Lines

cell sample	total HPV16 copies used in experiments	HPV16 copies/human genome (diploid)
JHU12	0	0
JHU13	0	0
JHU28	0	0
CasKi	187 502 400	600
SiHa	843 088	2
UM-SCC47	33 288 288	33
UM-SCC104	224 251	2
93-VU147T	51 201 008	68

2.4. Detection of HPV16 in a Commercially Synthesized Oligonucleotide Sequence and in Head and Neck Cancer Cell Lines. Impedance spectroscopy measurements were carried out with a Solartron model 1260 A (Solartron Analytical) in the range $1-10^6$ Hz, with the microfluidic chips coated with LbL films as described above. A commercially synthesized oligonucleotide sequence, analogous to a region of HPV16 DNA, was used as positive control as is referred to as ssDNA HPV16 (ssHPV16) positive control. Solutions of ssHPV16 (CTGTCCGGTTCTGCTTG), with concentrations 0.05, 0.1, 0.6, 1.1, 2.1, 3.1, 4.1, 5.1, and 6.1 nM were pumped into the microchannel at 22 and 55 °C during 10 min and flow rate of 12.5 μL/min, followed by washing with buffer solution for removal of poorly adsorbed molecules. After washing, the electrical measurements were performed with phosphate-buffered saline (PBS) injection into the microchannels, with flow rate 12.5 μL/min.

The electrical measurements of cancer cell samples were performed after the following procedure: cancer cell lines solutions (CasKi, SiHa, UM-SCC47, UM-SCC104, 93-VU147T, JHU12, JHU13, and JHU28) were injected into microfluidic electrode at 55 °C, followed by washing with PBS solution for the removal of poorly adsorbed molecules. Then, a PBS solution was injected into the microchannels with flow rate 12.5 μL/min to perform the electrical measurements.

As a negative control, a region of HPV18 DNA was used as a template to synthesize an oligonucleotide sequence referred to as ssDNA negative (ssNegative). The capacitance spectra were used to construct calibration curves by determining analytical parameters such as limit of detection, limit of quantification, and working range, in addition to adsorption studies of ssHPV16. The data could be used to determine the presence or absence of HPV16 in the head and neck cancer cell lines with previously known HPV status and viral copy.

2.5. Data Analysis. Detection experiments with sensors and biosensors using impedance spectroscopy normally lead to large amounts of multidimensional data, which are treated with statistical methods to reduce their dimensionality. For impedance or capacitance spectra, for example, this means that the whole spectrum—whose dimension can be ca. 70, which is the number of frequencies used in the measurements—is represented as a visual marker on the two-dimensional projected space. The techniques for such dimensionality reduction are referred to as multidimensional projection techniques, such as the principal component analysis (PCA) and interactive document mapping (IDMAP).[17] PCA employs linear combinations of the data attributes with which most of the data covariance can be accounted for. IDMAP, on the other hand, is an optimization, nonlinear technique that maps the data to the low-dimensional space with a strategy to minimize the error in the projection.[17,18] With IDMAP, the Euclidean distances calculated between different samples $X = \{x_1, x_2, x_3, ..., x_n\}$ in the original space are used to project the data instances onto a lower-dimension space, where $Y = \{y_1, y_2, y_3, ..., y_n\}$ is the position of the visual elements. The function employed to minimize the term $|\delta(x_i, x_j) - \mathrm{d}(f(x_i), f(x_j))| \; \forall \; x_i, x_j \in X$ is given in eq 2

$$S_{\text{IDMAP}} = \frac{\delta(x_i, x_j) - \delta_{\min}}{\delta_{\max} - \delta_{\min}} - \mathrm{d}(y_i, y_j) \quad (2)$$

where $\delta_{\max}$ and $\delta_{\min}$ are the maximum and minimum distances between data instances, respectively, $\delta(x_i, x_j)$ is the Euclidean distance between two samples in the original space and $\mathrm{d}(y_i, y_j)$ is the Euclidean distance on the projected space. In this work, IDMAP was applied using the PEx-Sensors software.[17,18]

3. RESULTS AND DISCUSSION

3.1. Microfluidic Electrode Modification and Genosensor Fabrication. The manufacture of biosensors with nanostructured films is advantageous owing to the versatility in the choice of materials, which may be combined synergistically to enhance sensitivity and selectivity. Because film adsorption on microfluidic devices is not as straightforward as on large substrates, a systematic study was performed with two experimental methods to characterize the nanostructured film of CHT and CS. Adsorption of the bilayers was monitored with a quartz crystal microbalance,[19] whose results are shown in Figure S1A,B in the Supporting Information. CHT and CS were found to adsorb onto the crystal surface within 3 and 2 min, respectively, upon electrostatic interaction between the protonated amino groups of CHT (NH_3^+) and the COO^- groups of CS. The mass adsorbed on the first bilayer was 1.38 μg/cm^2 of CHT and 3.71 μg/cm^2 of CS, whereas the second layer of CHT had a considerably larger mass (2.03 μg/cm^2) owing to the first CS layer that had a significant number of negative charges (COO^-), in comparison to the bare crystal. The mass of the second CS layer, on the other hand, did not differ much from the first, being 3.86 μg/cm^2. To warrant full deposition, the adsorption times adopted for fabricating the genosensor biosensor was 10 min for all layers.

Adsorption of CHT/CS layers on gold surfaces was confirmed with polarization-modulated infrared reflection-absorption spectroscopy (PM-IRRAS). One should recall that the band intensity in a PM-IRRAS spectrum depends not only on the amount of material adsorbed but also on the orientation of these groups with regard to the substrate surface. Under the experimental conditions used, upward bands mean that the dipole moments associated with the chemical groups are oriented perpendicular to the substrate surface. Figure 2 shows the normalized spectra of functionalized surfaces with CHT and CHT/CS (1–4 bilayers), featuring bands due to CHT at 1570 cm^{-1} (N–H and C–N in amide II) and 1418 cm^{-1} (CH_2 deformation)[20,21] and to CS at 1118 cm^{-1} (C–O vibrational stretching) and 1655 cm^{-1} (C═O angular deformation).[21−23] The intensity of the bands assigned to CS increases with the number of bilayers, indicating that the corresponding groups have their orientation preserved upon adsorption of further layers. For the bands due to CHT, on the other hand, the intensity does not vary with the number of deposited layers probably because as further CHT layers are adsorbed, the chemical groups responsible for the bands are reoriented.

The film architecture was designed for the cpHPV16 probe to hybridize with ssHPV16 or with DNA in HPV16$^+$ cells, thus warranting selectivity for the genosensor. The immobilization of the cpHPV16 probe was confirmed with the PM-IRRAS spectra of Figure 3A, where the spectrum of the Au surface was

DOI: 10.1021/acsami.8b14632
ACS Appl. Mater. Interfaces XXXX, XXX, XXX−XXX

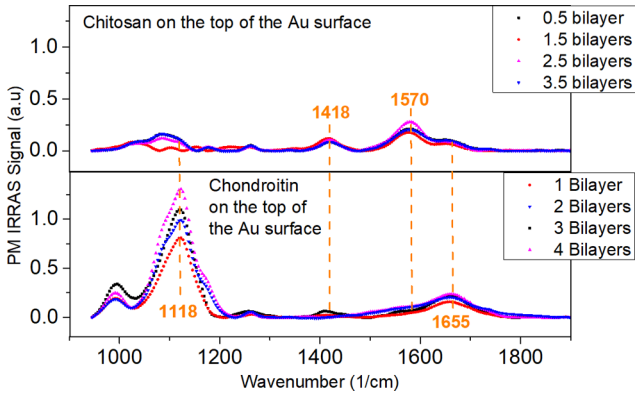

Figure 2. PM-IRRAS spectra for gold (Au) surfaces modified with LbL films of CHT and CHT/CS. When the top layer was made of CHT, the film was referred to as 0.5, 1.5, 2.5, and 3.5 bilayers (on the top chart). For CS on the top, the films had 1, 2, 3, and 4 bilayers, with the spectra shown on the chart on the bottom of the figure.

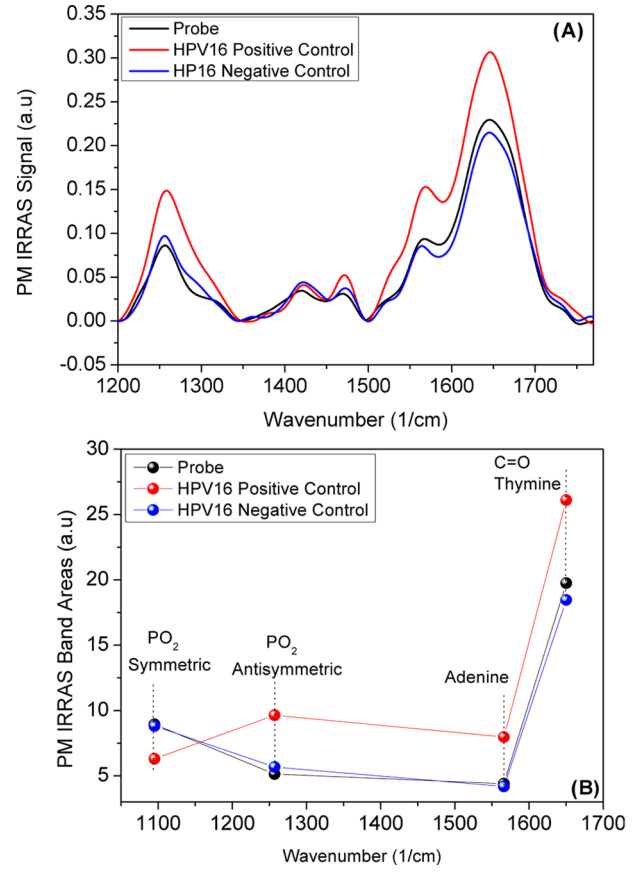

Figure 3. (A) Normalized PM-IRRAS spectra of CHT/CS films functionalized with probe (black line), probe/HPV16 negative (blue line) and probe/HPV16 positive (red line) to study the adsorption process. (B) PM-IRRAS band areas before (black/blue lines) and after hybridization (red line) at 55 °C.

taken as reference (the whole spectra are shown in Figure S2 in the Supporting Information). Also shown are the spectra that serve to identify the molecular-level interactions responsible for the hybridization and to illustrate the specificity toward ssHPV16. Hybridization of cpHPV16 probe and ssHPV16-positive control is inferred from the increase in the area under the bands in Figure 3B, including the antisymmetric PO_2 ($1255\ cm^{-1}$),[24] adenine ($1550\ cm^{-1}$),[25] and thymine carbonyl groups (C=O) ($1650\ cm^{-1}$).[26]

3.2. Detection of HPV16 at Different Concentrations of ssHPV16-Positive Control. The strong specific interaction between the immobilized probe chain (cpHPV16) and the complementary chain enables detection of the positive control (ssHPV16) with the impedance spectroscopy measurements using the microfluidic genosensor described in Section 2. Figure 4A,B display the capacitance spectra for the

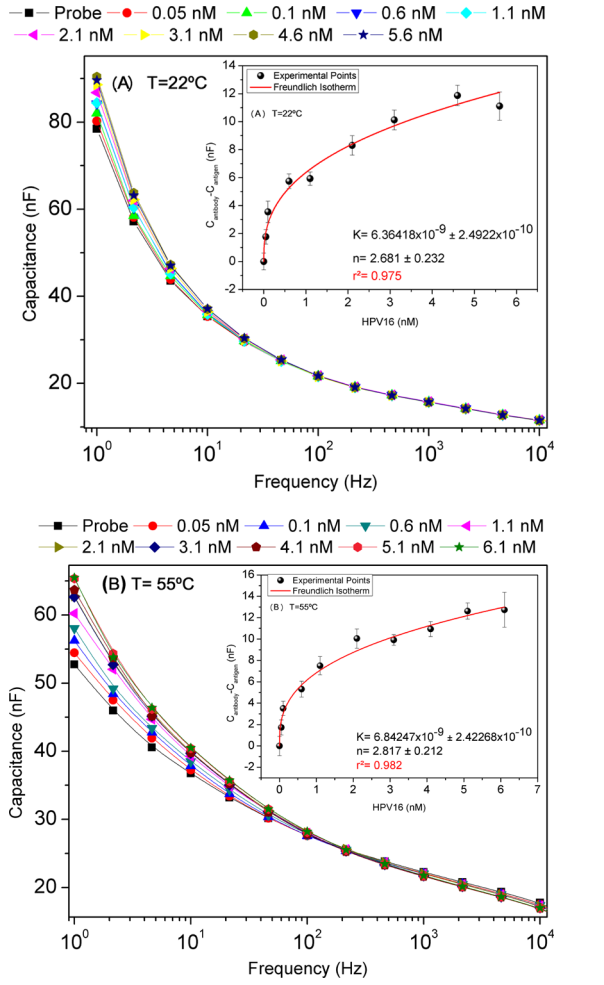

Figure 4. Capacitance spectra for genosensors immersed in phosphate-buffered saline (PBS) solution with different concentrations of ssHPV16-positive control at hybridization temperatures of (A) 22 °C and (B) 55 °C. The insets represent the calibration curves modeled with a Freundlich model.

genosensor exposed to different concentrations of ssHPV16 at 22 and 55 °C hybridization temperatures. Changes in the spectra are observed at frequencies below 100 Hz, in which modifications in the electrical double layer are induced by the molecular-level interactions. The changes are much larger for the hybridization temperature of 55 °C, which means that this is an optimized condition for genosensor fabrication. Calibration curves could be obtained by plotting the capacitance at 1 Hz versus concentration in the insets of Figure 4A,B. The limit of detection was calculated according to IUPAC recommendation (eq 3)[27] from the standard deviation of 10 reference curves and with α being the sensitivity obtained

DOI: 10.1021/acsami.8b14632
ACS Appl. Mater. Interfaces XXXX, XXX, XXX−XXX

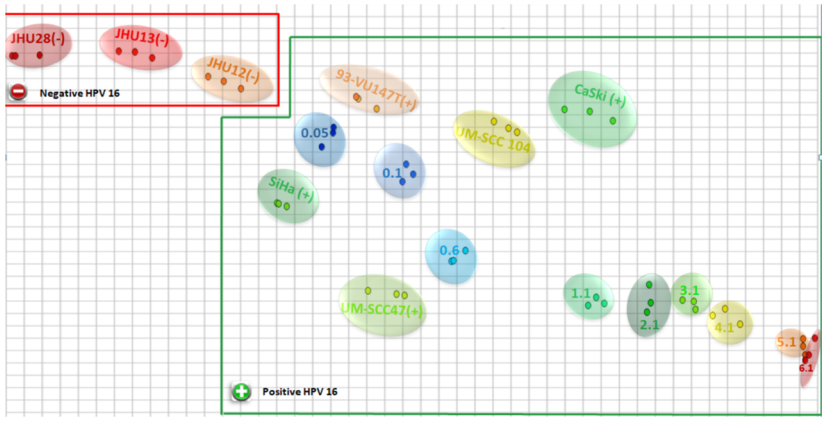

Figure 5. IDMAP plot obtained from the capacitance × frequency data of the commercially synthesized HPV16-positive control and the cell lines. The cell lines can be broadly clustered as negative (located to the left on the projection with a red line) and positive for HPV16 (located to the right with a green line).

from the angular coefficient of the linear part of the calibration curve.

$$\mathrm{LD} = \frac{3 \times \mathrm{SD}}{\alpha} \tag{3}$$

The limit of detection was 60.2 and 10.5 pM for the genosensors manufactured with hybridization temperatures of 22 and 55 °C, respectively. This performance is superior to other analytical devices to detect ssHPV16, such as the immunosensors made with carbon-printed electrodes modified with pyrrolidinylpeptides (4 nM),[28] immunosensors on Au electrodes modified with a L-cysteine thin film (18 nM),[29] and ssHPV16 genotyping test with a 16-electrode arrangement (100−200 pM).[30] With the optimized temperature of 55 °C, the working range of the genosensor is also extended, as the saturation of the signal (i.e., saturation of active sites due to irreversible interaction between ssHPV16-positive control and cpHVP16 probe[31]) occurs at 5.1 nM, in contrast to 4.6 nM for the hybridization temperature of 22 °C. The higher performance of the genosensor fabricated with hybridization at 55 °C was expected because this temperature corresponds to the optimized value for hybridization, whereas the temperature of 22 °C was used only for the purpose of comparison.

In addition to extracting analytical parameters from the genosensors, the calibration curves served to study the adsorption processes of ssHPV16 using the Freundlich model.[32−35] The adsorption of ssHPV16-positive control tended to level off when concentration reached 5 to 6 nM for the genosensors, with the concentration dependence being fitted using the Freundlich model (eq 4)

$$Q = K_a C^{1/n} \tag{4}$$

where Q is the change in capacitance, taken to be proportional to the amount of material adsorbed, K_a is an adsorption constant, C is the concentration of ssHPV16 in aqueous solution at equilibrium, and $(1/n)$ is a heterogeneity factor.[34,35] It should be noted that in an earlier work with immunosensors,[27] the adsorption process was better modeled with a Langmuir−Freundlich isotherm. Here, we also tested the Langmuir and Langmuir−Freundlich models, which could fit the data, but the accuracy in fitting was not as high as with the Freundlich model. The reason why the simple Freundlich and Langmuir−Freundlich models apply to adsorption processes of large molecules is probably the predominance of the specific interactions in the antibody−antigen pairs or in complementary DNA strands, which dominate over all the other interactions.

3.3. Validation of HPV16 Detection in Head and Neck Cancer Cell Lines. To validate the optimization of the genosensor manufacturing and verify the efficiency in HPV16 detection, the cervical cancer cell lines CaSki and SiHa and the head and neck cancer cell lines JHU12, JHU13, JHU28, UM-SCC47, UM-SCC104, and 93-VU147T were analyzed using information visualization maps obtained from the capacitance spectra of the cell lines and compared to the different dilutions of the ssHPV16-positive control. The electrical measurements were performed in blind tests and compared to the subsidiary information taken from other sources, such as HPV status and viral copy load. In the IDMAP projection in Figure 5, two clusters can be identified, in which ssHPV16-positive control concentration increases from left to right. The cell lines JHU12, JHU13, and JHU28 were correctly classified as "HPV16 negative" because they lack HPV16 genomic integration, whereas the remaining head and neck cell lines (UM-SCC47, UM-SCC104, and 93-VU147T) as well as CasKi and SiHa were classified as "HPV16 positive". The samples with the highest concentrations are clustered together owing to the saturation of the electrical signal, as seen in Figure 4. When the data for these samples are removed from the analysis, Figure S3 in the Supporting Information shows an even clearer distinction between the HPV16-positive and HPV16-negative samples. In summary, the genosensor is robust for detecting traces of HPV16 DNA in both ssHPV16-positive control and genomic DNA from the cell lines harboring integrated HPV16 genomes.

4. CONCLUSIONS

Microfluidic genosensors were produced with an LbL matrix of CHT and CS coated with a DNA probe to detect HPV16. The genosensors were shown to be chemically stable according to a few characterization techniques, including PM-IRRAS spectroscopy and quartz crystal microbalance. In commercial samples, they displayed high sensitivity with limit of detection of 60.2 and 10.5 pM for hybridization temperatures of 22 and 55 °C. This sensitivity is attributed to hybridization that resembles an adsorption process that could be fitted with a Freundlich isotherm and confirmed with PM-IRRAS spectroscopy. The genosensors were also highly selective, as

DOI: 10.1021/acsami.8b14632
ACS Appl. Mater. Interfaces XXXX, XXX, XXX−XXX

demonstrated in the analysis of the cell lines. Using a multidimensional projection technique, we were able to distinguish HPV16-positive from HPV16-negative head and neck cancer cell lines, in addition to distinguishing those from the synthetic ssDNA controls.

In summary, provided that the specificity of the genosensor is determined by the DNA sequence of the capture probe, genosensors can be specifically designed against particular DNA biomarkers for different tumor types, extending the use of this microfluidic genosensor platform to other diseases. The methods for detection and data analysis are entirely replicable and, owing to their simplicity and potential low cost, may be employed routinely in hospitals and even surgery centers, medical clinics, and doctor's offices.

■ ASSOCIATED CONTENT

Supporting Information

The Supporting Information is available free of charge on the ACS Publications website at DOI: 10.1021/acsami.8b14632.

Characterization of molecular architecture and control experiments (PDF)

■ AUTHOR INFORMATION

Corresponding Author

*E-mail: chu@ifsc.usp.br.

ORCID

Andrey Coatrini Soares: 0000-0003-4601-3555
Juliana Coatrini Soares: 0000-0001-5455-1770
Valquiria Cruz Rodrigues: 0000-0002-3738-3549
Matias Eliseo Melendez: 0000-0002-0643-6185
Rui Manuel Reis: 0000-0002-9639-7940
André Lopes Carvalho: 0000-0001-7214-6402
Osvaldo N. Oliveira, Jr.: 0000-0002-5399-5860

Notes

The authors declare no competing financial interest.

■ ACKNOWLEDGMENTS

The work was supported by CNPq (150985/2017-7), FAPESP (2013/14262-7), and Barretos Cancer Hospital. The authors are thankful to Dr. Antonio Riul Jr. (UNICAMP), Dr. Angelo Luiz Gobbi (LMF/CNPEM), and Maria Helena Piazzetta (LMF/CNPEM) for the microfluidic units and Dr. Flavio Makoto Shimizu (LMF/CNPEM) for the help in the analysis with adsorption models.

■ REFERENCES

(1) Ferlay, J.; Steliarova-Foucher, E.; Lortet-Tieulent, J.; Rosso, S.; Coebergh, J. W. W.; Comber, H.; Forman, D.; Bray, F. Cancer Incidence and Mortality Patterns in Europe: Estimates for 40 Countries in 2012. *Eur. J. Cancer* **2013**, *49*, 1374−1403.

(2) Jemal, A.; Bray, F.; Center, M. M.; Ferlay, J.; Ward, E.; Forman, D. Global Cancer Statistics. *Ca-Cancer J. Clin.* **2011**, *61*, 69−90.

(3) Wong, D. T. W.; Todd, R.; Tsuji, T.; Donoff, R. B. Molecular Biology of Human Oral Cancer. *Crit. Rev. Oral Biol. Med.* **1996**, *7*, 319−328.

(4) Mashberg, A.; Boffetta, P.; Winkelman, R.; Garfinkel, L. Tobacco Smoking, Alcohol Drinking, and Cancer of the Oral Cavity and Oropharynx among U.S. Veterans. *Cancer* **1993**, *72*, 1369−1375.

(5) Spence, T.; Bruce, J.; Yip, K.; Liu, F.-F. HPV Associated Head and Neck Cancer. *Cancers* **2016**, *8*, No. 75.

(6) Ang, K. K.; Harris, J.; Wheeler, R.; Weber, R.; Rosenthal, D. I.; Nguyen-Tân, P. F.; Westra, W. H.; Chung, C. H.; Jordan, R. C.; Lu, C.; Kim, H.; Axelrod, R.; Silverman, C. C.; Redmond, K. P.; Gillison, M. L. Human Papillomavirus and Survival of Patients with Oropharyngeal Cancer. *N. Engl. J. Med.* **2010**, *363*, 24−35.

(7) Shi, W.; Kato, H.; Perez-Ordonez, B.; Pintilie, M.; Huang, S.; Hui, A.; O'Sullivan, B.; Waldron, J.; Cummings, B.; Kim, J.; Ringash, J.; Dawson, L. A.; Gullane, P.; Siu, L.; Gillison, M.; Liu, F. F. Comparative Prognostic Value of HPV16 E6 MRNA Compared with in Situ Hybridization for Human Oropharyngeal Squamous Carcinoma. *J. Clin. Oncol.* **2009**, *27*, 6213−6221.

(8) Frías, I. A. M.; Avelino, K. Y. P. S.; Silva, R. R.; Andrade, C. A. S.; Oliveira, M. D. L. Trends in Biosensors for HPV: Identification and Diagnosis. *J. Sens.* **2015**, *2015*, 1−16.

(9) Piccoli, J.; Hein, R.; El-Sagheer, A. H.; Brown, T.; Cilli, E. M.; Bueno, P. R.; Davis, J. J. Redox Capacitive Assaying of C-Reactive Protein at a Peptide Supported Aptamer Interface. *Anal. Chem.* **2018**, *90*, 3005−3008.

(10) Ariga, K.; Yamauchi, Y.; Rydzek, G.; Ji, Q.; Yonamine, Y.; Wu, K. C.-W.; Hill, J. P. Layer-by-Layer Nanoarchitectonics: Invention, Innovation, and Evolution. *Chem. Lett.* **2014**, *43*, 36−68.

(11) Ariga, K.; Minami, K.; Shrestha, L. K. Nanoarchitectonics for Carbon-Material-Based Sensors. *Analyst* **2016**, *141*, 2629−2638.

(12) Rydzek, G.; Ji, Q.; Li, M.; Schaaf, P.; Hill, J. P.; Boulmedais, F.; Ariga, K. Electrochemical Nanoarchitectonics and Layer-by-Layer Assembly: From Basics to Future. *Nano Today* **2015**, *10*, 138−167.

(13) Decher, G.; Schlenoff, J. B. *Multilayer Thin Films: Sequential Assembly of Nanocomposite Materials*; Wiley-VCH: Weinheim, 2012.

(14) Decher, G.; Hong, J. D.; Schmitt, J. Buildup of Ultrathin Multilayer Films by a Self-Assembly Process: III. Consecutively Alternating Adsorption of Anionic and Cationic Polyelectrolytes on Charged Surfaces. *Thin Solid Films* **1992**, *210−211*, 831−835.

(15) Soares, J. C.; Shimizu, F. M.; Soares, A. C.; Caseli, L.; Ferreira, J.; Oliveira, O. N. Supramolecular Control in Nanostructured Film Architectures for Detecting Breast Cancer. *ACS Appl. Mater. Interfaces* **2015**, *7*, 11833−11841.

(16) Arantes, L. M. R. B.; de Carvalho, A. C.; Melendez, M. E.; Centrone, C. C.; Góis-Filho, J. F.; Toporcov, T. N.; Caly, D. N.; Tajara, E. H.; Goloni-Bertollo, E. M.; Carvalho, A. L. Validation of Methylation Markers for Diagnosis of Oral Cavity Cancer. *Eur. J. Cancer* **2015**, *51*, 632−641.

(17) Paulovich, F. V.; Moraes, M. L.; Maki, R. M.; Ferreira, M.; Oliveira, O. N., Jr.; de Oliveira, M. C. F. Information Visualization Techniques for Sensing and Biosensing. *Analyst* **2011**, *136*, 1344−1350.

(18) Paulovich, F. V.; Maki, R. M.; de Oliveira, M. C. F.; Colhone, M. C.; Santos, F. R.; Migliaccio, V.; Ciancaglini, P.; Perez, K. R.; Stabeli, R. G.; Perinoto, Â. C.; Oliveira, O. N., Jr.; Zucolotto, V. Using Multidimensional Projection Techniques for Reaching a High Distinguishing Ability in Biosensing. *Anal. Bioanal. Chem.* **2011**, *400*, 1153−1159.

(19) Sauerbrey, G. Verwendung von Schwingquarzen zur Wägung dünner Schichten und zur Mikrowägung. *Z. Phys.* **1959**, *155*, 206−222.

(20) Barth, A. The Infrared Absorption of Amino Acid Side Chains. *Prog. Biophys. Mol. Biol.* **2000**, *74*, 141−173.

(21) Colthup, N. B.; Daly, L. H.; Wiberley, S. E. *Introduction to Infrared and Raman Spectroscopy*, 3rd ed.; Academic Press: Boston, 1990.

(22) Akhshabi, S.; Biazar, E.; Singh, V.; Keshel, S. H.; Nagaraja, G. The Effect of Glutaraldehyde Cross-Linker on Structural and Biocompatibility Properties of Collagen-Chondroitin Sulfate Electrospun Mat. *Mater. Technol.* **2018**, *33*, 253−261.

(23) Więckowski, A., Korzeniewski, C., Braunschweig, B. *Vibrational Spectroscopy at Electrified Interfaces*; Wiley: Hoboken, New Jersey, 2013.

(24) Zelig, U.; Mordechai, S.; Shubinsky, G.; Sahu, R. K.; Huleihel, M.; Leibovitz, E.; Nathan, I.; Kapelushnik, J. Pre-Screening and Follow-up of Childhood Acute Leukemia Using Biochemical Infrared Analysis of Peripheral Blood Mononuclear Cells. *Biochim. Biophys. Acta, Gen. Subj.* **2011**, *1810*, 827−835.

DOI: 10.1021/acsami.8b14632
ACS Appl. Mater. Interfaces XXXX, XXX, XXX−XXX

(25) Alex, S.; Dupuis, P. FT-IR and Raman Investigation of Cadmium Binding by DNA. *Inorg. Chim. Acta* **1989**, *157*, 271−281.
(26) Marty, R.; N'soukpoe-Kossi, C. N.; Charbonneau, D.; Weinert, C. M.; Kreplak, L.; Tajmir-Riahi, H.-A. Structural Analysis of DNA Complexation with Cationic Lipids. *Nucleic Acids Res.* **2009**, *37*, 849−857.
(27) Thapa, A.; Soares, A. C.; Soares, J. C.; Awan, I. T.; Volpati, D.; Melendez, M. E.; Fregnani, J. H. T. G.; Carvalho, A. L.; Oliveira, O. N. Carbon Nanotube Matrix for Highly Sensitive Biosensors To Detect Pancreatic Cancer Biomarker CA19-9. *ACS Appl. Mater. Interfaces* **2017**, *9*, 25878−25886.
(28) Jampasa, S.; Wonsawat, W.; Rodthongkum, N.; Siangproh, W.; Yanatatsaneejit, P.; Vilaivan, T.; Chailapakul, O. Electrochemical Detection of Human Papillomavirus DNA Type 16 Using a Pyrrolidinyl Peptide Nucleic Acid Probe Immobilized on Screen-Printed Carbon Electrodes. *Biosens. Bioelectron.* **2014**, *54*, 428−434.
(29) Campos-Ferreira, D. S.; Nascimento, G. A.; Souza, E. V. M.; Souto-Maior, M. A.; Arruda, M. S.; Zanforlin, D. M. L.; Ekert, M. H. F.; Bruneska, D.; Lima-Filho, J. L. Electrochemical DNA Biosensor for Human Papillomavirus 16 Detection in Real Samples. *Anal. Chim. Acta* **2013**, *804*, 258−263.
(30) Civit, L.; Fragoso, A.; O'Sullivan, C. K. Electrochemical Biosensor for the Multiplexed Detection of Human Papillomavirus Genes. *Biosens. Bioelectron.* **2010**, *26*, 1684−1687.
(31) Soares, A. C.; Soares, J. C.; Shimizu, F. M.; Melendez, M. E.; Carvalho, A. L.; Oliveira, O. N. Controlled Film Architectures to Detect a Biomarker for Pancreatic Cancer Using Impedance Spectroscopy. *ACS Appl. Mater. Interfaces* **2015**, *7*, 25930−25937.
(32) Badruzzaman, M.; Westerhoff, P.; Knappe, D. R. U. Intraparticle Diffusion and Adsorption of Arsenate onto Granular Ferric Hydroxide. *Water Res.* **2004**, *38*, 4002−4012.
(33) Lin, T.-F.; Wu, J.-K. Adsorption of Arsenite and Arsenate within Activated Alumina Grains: Equilibrium and Kinetics. *Water Res.* **2001**, *35*, 2049−2057.
(34) Wang, C.; Boithias, L.; Ning, Z.; Han, Y.; Sauvage, S.; Sánchez-Pérez, J.-M.; Kuramochi, K.; Hatano, R. Comparison of Langmuir and Freundlich Adsorption Equations within the SWAT-K Model for Assessing Potassium Environmental Losses at Basin Scale. *Agric. Water Manag.* **2017**, *180*, 205−211.
(35) Dada, A. O.; Olalekan, A. P.; Olatunya, A. M.; Dada, O. Langmuir, Freundlich, Temkin and Dubinin−Radushkevich Isotherms Studies of Equilibrium Sorption of Zn2 + Unto Phosphoric Acid Modified Rice Husk. *IOSR J. Appl. Chem.* **2012**, *3*, 38−45.

DOI: 10.1021/acsami.8b14632
ACS Appl. Mater. Interfaces XXXX, XXX, XXX−XXX